Fine structure and selection rules for excitonic transitions in silicon nanostructures

M. Dovrat,[1] Y. Shalibo,[1] N. Arad,[1] I. Popov,[1] S.-T. Lee,[2] and A. Sa'ar[1,*]

[1]*Racah Institute of Physics and the Center for Nanoscience and Nanotechnology, The Hebrew University of Jerusalem, Jerusalem 91904, Israel*

[2]*Center for Super-Diamond and Advanced Films and Department of Physics and Materials Science, City University of Hong Kong, Hong Kong SAR, China*

(Received 9 January 2009; published 10 March 2009)

The excitonic fine structure, including splitting due to direct and exchange interactions, has experimentally been resolved from silicon nanocrystals and from silicon nanorods. We have found the hierarchy of levels for silicon nanorods to be different from that of silicon nanocrystals with the slower semidark state located above the faster semibright state. The results are analyzed in terms of spin and orbital selection rules indicating that the dimensionality of the exciton determines the relative contribution of the direct Coulomb and the exchange interactions in these nanostructures.

DOI: 10.1103/PhysRevB.79.125306 PACS number(s): 71.35.−y, 73.22.−f, 78.55.−m, 78.67.−n

Optical spectroscopy of excitonic transitions in semiconductor nanostructures is a powerful tool for studying basic interactions between electron-hole pairs in the strong confinement regime where the size of the nanostructure is smaller or comparable to the Bohr radius of the exciton.[1] The Coulomb interaction that binds electron-hole pairs may also give rise to a splitting of the excitonic states according to the spin configuration of the carriers. For example, the exchange interaction can split the multiplet state of the exciton into upper, optically allowed, bright state and lower, optically forbidden, dark state. Strong confinement of the exciton in small nanostructures enhances the excitonic splitting as experimentally observed for both direct-gap[2] and indirect-gap[3,4] semiconductor nanostructures. In most experiments reported so far,[5,6] the experimental data are analyzed in terms of a simple singlet-triplet model[7] where the degeneracy of the two spin 1/2 particles (e.g., the electron and the hole) is lifted by the exchange interaction, giving rise to lower ($S=1$) triplet state and an upper ($S=0$) singlet state. Yet, this simplified picture ignores profound characteristics of the nanostructures such as the properties of the bulk semiconductor, its degeneracy, and the orbital angular momentum of the carriers.[8,9] In particular, for silicon nanostructures the electrons and the holes originate from different orbitals and symmetry points of the Brillouin zone and therefore, these characteristics of the carriers together with the shape and the symmetry of the nanostructures should be manifested in the fine structure of the exciton exchange splitting pattern.

In this work, we experimentally resolve the fine structure of the excitonic exchange splitting pattern for silicon nanocrystals (SiNCs) and silicon nanorods (SiNRs) with the surprising observation of a different level's hierarchy for SiNRs where the slower semidark exciton state being at the midenergy level rather than the lower energy level as in the case of SiNCs. Our analysis indicates that in one-dimensional (1D) Si nanostructures (e.g., SiNRs) the direct Coulomb interaction dominates over the exchange interaction and is essentially responsible to the fine structure of the exchange splitting pattern, as opposed to zero-dimensional (0D) (SiNCs) where the exchange interaction dominates over the direct interaction. We analyze these results in terms of spin and orbital selection rules, reflecting the more complex structure of the excitonic levels in silicon nanostructures.

SiNCs were grown on top of (100) p-type silicon wafer by serial deposition of thin Si and SiO_2 layers using RF magnetron sputtering followed by high-temperature ($T=1150\ ^\circ C$) annealing in nitrogen atmosphere.[6] 30 periods consisting of 10 nm SiO_2 and a silicon layer with thicknesses varying between 2–5 nm have been deposited. For the growth of SiNRs (Ref. 10) we have used the oxide-assisted growth method reported elsewhere.[11,12] This growth method creates fairly long (few microns) core-shell silicon nanowires with inner silicon core of about 10–30 nm in diameter and outer SiO_2 shell with a diameter in the range of 20–50 nm. In a recent study we have found that the blue-green photoluminescence (PL) from these as-grown, moderate-size silicon nanowires is not related to quantum size effects but rather to interface states and oxide defects.[13] In order to approach the strong confinement regime we have applied the following procedure. At first, the as-grown nanowires were etched by aqueous hydrofluoric (HF) solution for 10 min to remove the oxide shell. Next, the samples were dry oxidized for 2.5–3.5 h at a temperature of $T=700\ ^\circ C$. This low oxidation temperature ensures slow oxidation rate and a good control of the silicon core diameter down to the few nanometers (in diameter) range. Figure 1 presents cross-section TEM images of typical samples; in Fig. 1(a) few periods of SiNCs superlattice, with average diameter of about 4 nm, are shown while Fig. 1(b) reveals a small silicon nanorod, 3.5 nm in diameter and about 30 nm in length, obtained after 180 min of oxidation. The inset to Fig. 1(b) reveals the {111} crystal planes of silicon, which is the preferred crystallographic direction of most SiNRs, and has been obtained after filtering the corresponding image of the SiNR in the frequency domain. Both silicon nanostructures are embedded in the amorphous phase of SiO_2. Room-temperature PL spectra (excited with Ar^+ ion laser operating at 488 nm) of both samples are shown in Fig. 2. For SiNRs a red-emission band appears after 150 min of oxidation and is monotonically blueshifted with the increasing time of oxidation[14] as expected in the quantum confinement regime.[12,15] Similarly, we have observed a monotonic blueshift of the PL with the decreasing

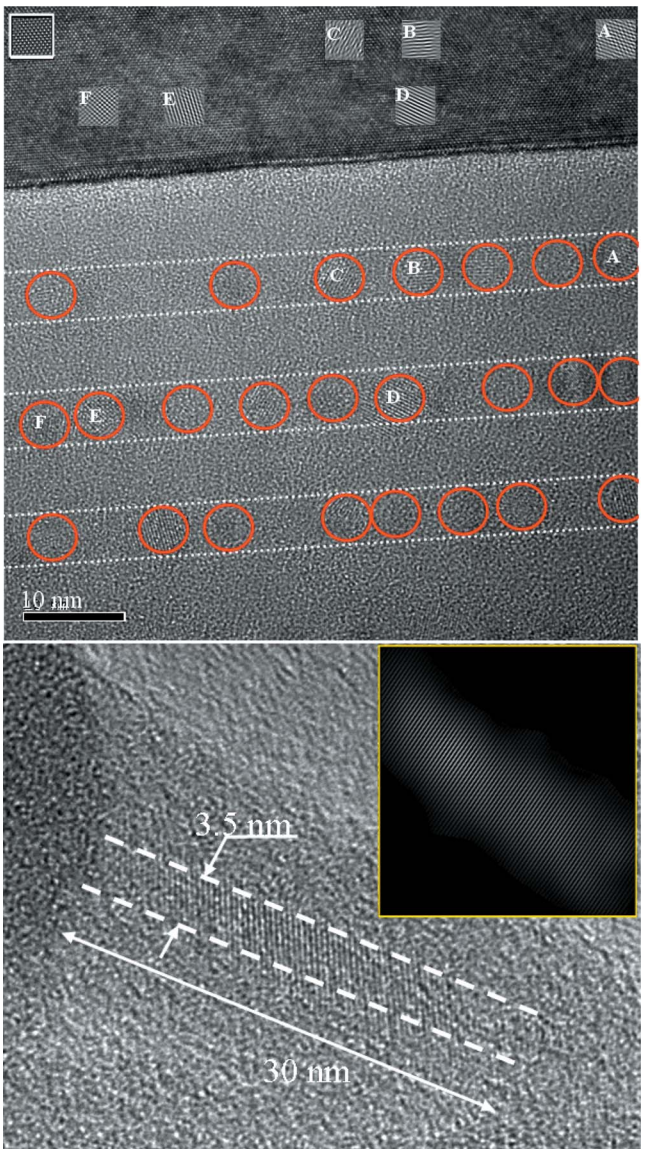

FIG. 1. (Color online) HRTEM images revealing (top) three layers of SiNCs, marked by dashed white lines, embedded in the amorphous phase of SiO_2. The SiNCs are marked by circles. The insets A, B, C, D, E and F are few representative images of the silicon crystal planes, obtained by filtering the corresponding images of the nanocrystals in the frequency domain. (bottom) The same for a crystalline silicon nanorod coated by amorphous SiO_2 with the inset showing the crystal planes of the nanorod after filtering.

average size of the SiNCs in a very good agreement with other reports on similar SiNCs.[16]

Next, let us describe results obtained by time-resolved PL spectroscopy. Details of the experimental setup are described elsewhere.[6,13] The PL decay curves for all samples, temperatures and wavelengths follow a stretched-exponential decay function, $I/I_0 \cong \exp[-(t/\tau)^{\beta}]$, in a good agreement with the temporal behavior found by us[6] and by others[4,14] for similar silicon nanostructures.[17] The inset to Fig. 3(b) shows typical decay curves from which, the PL decay times, τ, have been extracted. Similar to other reports,[4–7] we have found a strong dependence of the PL lifetime on temperature. However,

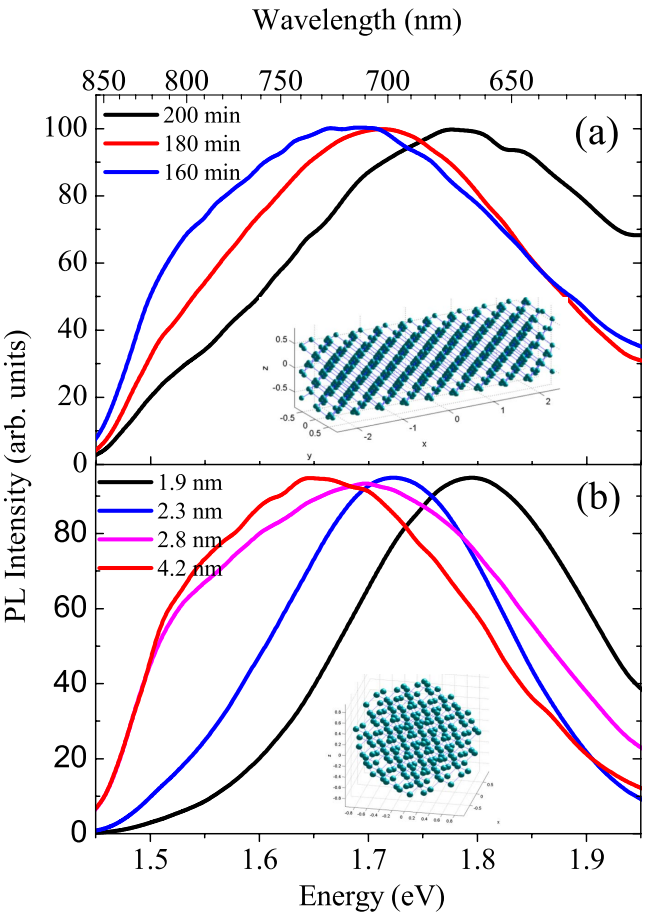

FIG. 2. (Color online) Room-temperature photoluminescence spectra from (a) SiNRs after different times of oxidation and (b) superlattices of SiNCs with different diameters. The insets show the models for SiNRs and SiNCs used to derive the symmetries of the structures.

while for SiNCs we find a monotonic increase in τ upon cooling (i.e., slower PL decay times at lower temperatures) until it saturates at temperatures below 20–30 K, for SiNRs the PL decay time shows a local maximum at temperatures ~60–70 K followed by a saturation below ~30 K for all samples and photon energies; see Fig. 3(a). In addition, we have found that the PL is quenched at temperatures below 6 K for both samples. This range of temperatures is marked by the dashed areas in Fig. 3 where we could not resolve the decay time.[18]

The above behavior of the PL decay time cannot be explained by a simple two-level model such as the singlet-triplet model.[5–7] Instead, we find the experimental data to fit a three-level model [schematically shown in the inset to Fig. 3(a)] where the PL decay time is determined by the relative population of the excitonic levels according to the following expression:

$$\frac{1}{\tau} = \frac{g_1/\tau_1 + (g_2/\tau_2)\exp(-\Delta_{21}/kT) + (g_3/\tau_3)\exp(-\Delta_{31}/kT)}{g_1 + g_2\exp(-\Delta_{21}/kT) + g_3\exp(-\Delta_{31}/kT)}, \quad (1)$$

where Δ_{ij} is the splitting energy between the ith and the jth levels, τ_j and g_j are the lifetime and the corresponding de-

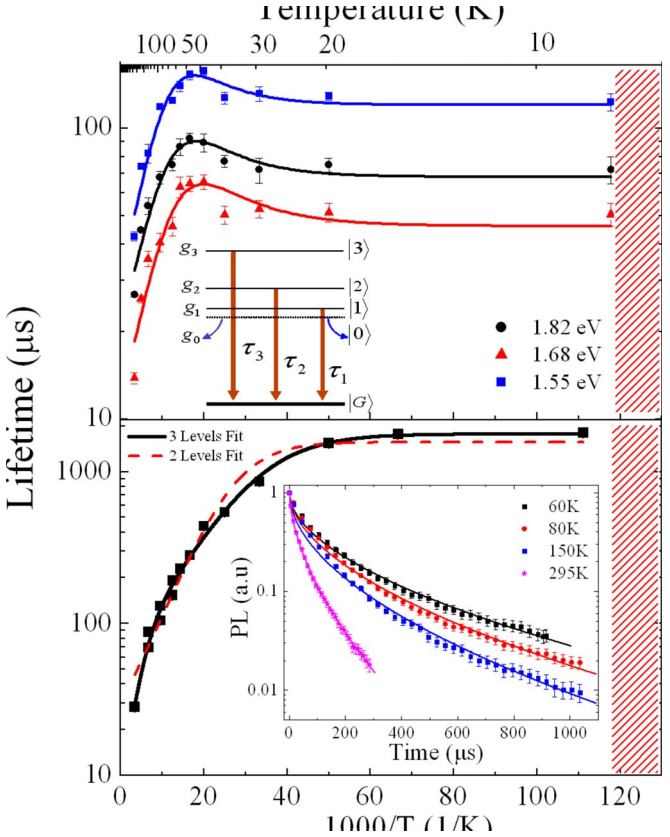

FIG. 3. (Color online) The measured PL lifetime (symbols) versus the inverse temperature for (a) SiNRs after 180 min of oxidation at several photon energies. The solid lines represent the best fit the data to the three-level model of Eq. (1). The inset is a simple scheme of the four excitonic levels (plus the ground state of no excitons) and the allowed optical transitions. (b) The PL lifetime for SiNCs with average diameter of 2.3 nm at photon energy of 1.72 eV. The black solid line represents the best fit of the data to a three-level model while the red line represents the best fit to a two-level model. In both figures, the red dashed areas represent the range of low temperatures where the PL is quenched.

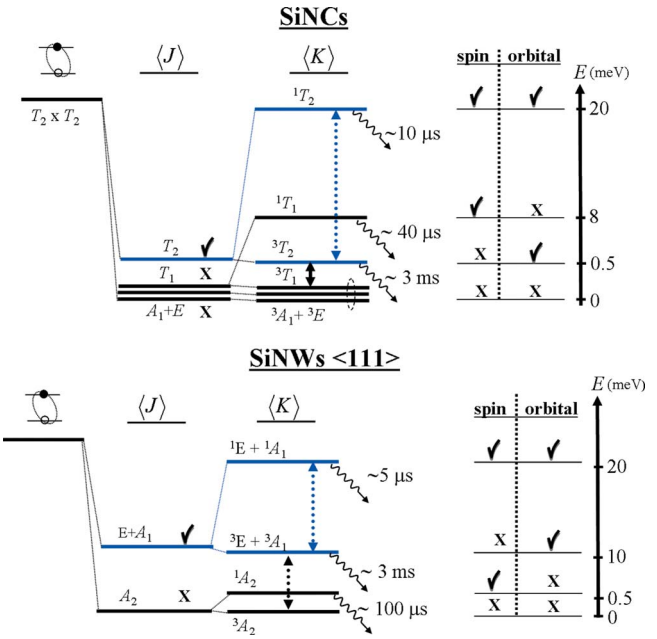

FIG. 4. (Color online) Schematic illustration of the excitonic fine structure for (a) SiNCs and (b) SiNRs oriented along the ⟨111⟩ direction. From left to right we present the excitonic levels neglecting both the direct and the exchange interactions ($T_2 \times T_2$), splitting due to direct interaction $\langle J \rangle$ and finally, the excitonic pattern after introducing the exchange interaction, $\langle K \rangle$. For comparison, the measured energies and lifetimes of the upper three excitonic states are presented. The corresponding spin and orbital selection rules for each level are presented in the table on the right sides. The level's notations are explained in the text. The vertical dashed arrows indicate the measured splitting due to exchange interaction (blue) and due to direct interaction (black).

generacy of the jth level, respectively, and T is the temperature. Let us emphasize that Eq. (1) (i.e., the three-level model) should be utilized to both SiNCs and SiNRs. For SiNRs it means that the lowest energy level, which is the only populated level at low temperatures, has a moderate lifetime, $\tau_1 \approx 50-150$ μsec. Upon heating, the second level becomes populated. Therefore, the local maximum of the PL decay time indicates that this level is characterized by the slowest lifetime, $\tau_2 \approx 2-4$ msec. Further heating of the SiNRs gives rise to a thermal population of the third level that is characterized by the fastest lifetime, $\tau_3 \approx 2-8$ μsec, and is responsible to the faster PL decay times upon heating to temperatures above ~70 K.

For SiNCs the PL decay time increases monotonically with the decreasing temperature. Yet, here we also find the three-level model to be the proper model for describing the PL decay time. Figure 3(b) shows a comparison obtained by fitting the experimental data either to the three-level model (black line) or to the two-level model (red dashed line). Evidently, we find the three-level model to fit much better for all samples and photon energies. From these fits we find that the lower energy level is characterized by the slowest lifetime, $\tau_1 \approx 2-4$ msec, the midlevel has a moderate lifetime, $\tau_2 \approx 20-60$ μsec, and the upper level is characterized, again, by the fastest lifetime, $\tau_3 \approx 5-15$ μsec. Notice that this hierarchy of the excitonic levels means that there is no local maximum of the decay time since, upon heating, faster levels are populated giving rise to a monotonic decrease in the PL lifetime as observed in our experiments. For reasons to be explained hereafter, we have used the following degeneracy factors for the fittings: $(g_1:g_2:g_3)=9:3:3$ and $=1:24:8$ for SiNCs and SiNRs, respectively. In Fig. 4, we schematically show the fine structure of the excitonic splitting pattern for both SiNCs and SiNRs where the splitting energies and the lifetimes were taken to be the average values of these parameters. In addition, the PL quenching at temperatures below 6 K suggests an additional splitting of the lower level (for both SiNCs and SiNRs) with the ground energy level being a dark state. The splitting energy between the ground excitonic states [marked $|0\rangle$ and $|1\rangle$ at the inset to Fig. 3(a)] has been estimated to be $\leq 400-600$ μeV.

To follow the origin of this surprising phenomenon of a different level's hierarchy associated with a change in the dimensionality of the exciton, let us notice that the excitonic spectra have been calculated by several groups for

SiNCs.[8,9,19–21] Following Reboredo *et al.*,[8] we suggest that the structure of the excitonic splitting pattern (for SiNCs) can be explained by utilizing spin and orbital selection rules. We notice that the symmetry of the exciton can be derived from symmetries of the bulk silicon carriers (i.e., conduction electrons and valence holes). These particles are characterized by the T_2 symmetry of the bulk silicon T_d point group. Therefore, we find $T_2 \times T_2 = T_1 + T_2 + E + A_1$ where T_1, T_2, E, and A_1 are the irreducible representations of the T_d point group for a spherical exciton. Within the electric dipole approximation, only T_2 (which is the "vectorlike" representation) represents optically active excitonic states for which optical transitions into the ground state (i.e., no excitons) are allowed. Reboredo *et al.*[8] showed that the direct Coulomb interaction already lifts the degeneracy of the exciton, forming four subgroups of levels accordingly. Introducing the exchange interaction further splits these subgroups into singlets and triplets and finally, configuration mixing (e.g., off-diagonal interactions) provides the final spectrum of the excitonic fine structure. Our measurements agree very well with this picture. Furthermore, we can provide now a simple and elegant explanation to the hierarchy of the excitonic splitting and lifetimes for SiNCs. The lowest excitonic group consists of four states ($^3T_1, ^3A_1, ^3E$) with a total degeneracy of 18. Optical transitions from this subgroup are both spin and orbitally forbidden (as all states are spin triplet and none of them contain the T_2 symmetry). Hence, this group of states can be identified as the measured dark exciton. The higher subgroups of semidark and semibright excitonic states include the $^3T_2$ level (nine times folded degeneracy) that is orbitally allowed but spin forbidden, the $^1T_1$ level (three times folded degeneracy) that is orbitally forbidden but spin allowed and finally, the upper $^1T_2$ level (three times folded degeneracy) that is both orbitally and spin allowed. We notice that one should expect a significantly weaker relaxation of the spin selection rules (mainly due to spin-orbit interaction, which is fairly weak in silicon[22]) relative to the orbital selection rules that can relax by deviations from sphericity, structural imperfections, surface and interface defects.[23,24] This provides a nice explanation to the hierarchy of lifetimes as measured in our experiments for SiNCs; see Fig. 4(a).

Turning to SiNRs,[25] let us apply similar arguments to excitons in a cylindrical geometry.[26] Here, we have found that a similar (but not identical) hierarchy can be derived only for SiNRs grown along the ⟨100⟩ direction (D_{2d} point symmetry), the ⟨111⟩ (C_{3v} symmetry) and the ⟨110⟩ (C_{2v} symmetry) directions. For other directions of lower symmetry, such as the ⟨112⟩ direction (C_S symmetry), one cannot derive similar selection rules for the excitonic levels. For example, let us consider selection rules for ⟨111⟩ oriented SiNRs [inset to Fig. 2(a)] as most nanorods in our samples are oriented along this direction; see Fig. 1(b). In this case, optically active excitons are related to the $(E+A_1)$ irreducible representations (e.g., vectorlike representations). Here again, the ground dark exciton state is composed of those states that are spin forbidden (triplets) and do not contain E or A_1 symmetries. The results shown in Fig. 4(b) suggest that the lower $^1A_2$ level is spin allowed but orbitally forbidden state while the upper $^3E + ^3A_1$ group of states consists of spin forbidden but orbitally allowed levels. Similar hierarchy can be obtained for the other directions of high symmetry. Hence, we conclude that the interchange of the excitonic levels hierarchy for SiNRs is related to the corresponding swap between spin forbidden and orbitally allowed states (relative to those of SiNCs).

To understand the origin of this phenomenon, let us estimate the relative contribution of the direct Coulomb (J) and the exchange (K) interactions to the excitonic energies. These contributions can be estimated as follows. For SiNCs (SiNRs) we take the energy splitting between the T_2 $(E+A_1)$, orbitally allowed singlet-triplet states as an estimate of the exchange energy, $\langle K \rangle$. This conclusion is based on the observation that the direct Coulomb interaction does not contribute to this splitting. On the other hand, as the triplet states of the T_2 and the T_1 levels ($E+A_1$ and A_2 for SiNRs) are essentially insensitive to the exchange interaction, we take the energy difference between these levels as an estimate of the splitting energy caused by the direct term, $\langle \Delta J \rangle$. From the experimental results (see Fig. 4) we can now evaluate the ratio of these terms in 0D (SiNCs) and in 1D (SiNRs);[27]

$$\frac{\langle K/\Delta J \rangle_{0D}}{\langle K/\Delta J \rangle_{1D}} \approx 40 \pm 20. \tag{2}$$

We conclude that in 0D the larger exchange splitting of orbitally allowed states causes the spin forbidden state ($^3T_2$) to fall below the spin allowed state ($^1T_1$). In 1D (SiNRs), however, the smaller exchange splitting of orbitally allowed states does not give rise to an interchange of the spin forbidden ($^3E + ^3A_1$) and the spin allowed ($^1A_2$) states. We can point out few possible mechanisms that could be responsible to this result. For example, it has been suggested that the long-range exchange interaction[28] plays a more profound role in 0D whereas dielectric screening is less efficient in 1D. It has also been suggested that the exchange energy is more sensitive to quantum confinement of the carriers than the direct Coulomb energy.[19] Yet, further investigation based on first-principles calculations, which is beyond the scope of this work, is required to verify the origin of this phenomenon.

In summary, we have revealed the fine structure of the exciton in silicon nanostructures, showing that it consists of a ground dark state, upper semidark and semibright states and finally upper bright state. Yet, for SiNRs the slowest semidark state falls above the faster semibright state as opposed to SiNCs. We assign this phenomenon to the role of direct and exchange interactions where the larger exchange interaction in 0D swaps the spin forbidden and orbitally allowed states whereas in 1D, the smaller exchange to direct energies ratio does not allow such a phenomenon.

This work was supported by a joint Chinese-Israeli research grant provided by the ministries of Science of both countries and by a grant of the Israel Science Foundation (ISF).

*Corresponding author: saar@vms.huji.ac.il

[1] G. D. Scholes and G. Rumbles, Nature Mater. **5**, 683 (2006).
[2] M. Nirmal, D. J. Norris, M. Kuno, M. G. Bawendi, A. L. Efros, and M. Rosen, Phys. Rev. Lett. **75**, 3728 (1995); M. Bayer *et al.*, Phys. Rev. B **65**, 195315 (2002); N. Le Thomas, E. Herz, O. Schops, and U. Woggon, Phys. Rev. Lett. **94**, 016803 (2005); C. de Mello Donegá, M. Bode, and A. Meijerink, Phys. Rev. B **74**, 085320 (2006).
[3] M. Nirmal, D. J. Norris, M. Kuno, M. G. Bawendi, A. L. Efros, and M. Rosen, Phys. Rev. Lett. **75**, 3728 (1995).
[4] J. Linnros, N. Lalic, A. Galeckas, and V. Grivickas, J. Appl. Phys. **86**, 6128 (1999); X. Wen, L. V. Dao, and P. Hannaford, J. Phys. D **40**, 3573 (2007); S. Kim, Y. M. Park, S.-H. Choi, K. J. Kim, and D. H. Choi, *ibid.* **40**, 1339 (2007); F. Trojánek, K. Neudert, M. Bittner, and P. Malý, Phys. Rev. B **72**, 075365 (2005).
[5] J. Diener, D. I. Kovalev, G. Polisski, and F. Koch, Appl. Phys. Lett. **74**, 3350 (1999); A. Y. Kobitski, K. S. Zhuravlev, H. P. Wagner, and D. R. T. Zahn, Phys. Rev. B **63**, 115423 (2001); M. L. Brongersma, P. G. Kik, A. Polman, K. S. Min, and H. A. Atwater, Appl. Phys. Lett. **76**, 351 (2000); S. Luttjohann, C. Meier, M. Offer, A. Lorke, and H. Wiggers, Europhys. Lett. **79**, 37002 (2007).
[6] M. Dovrat, Y. Goshen, J. Jedrzejewski, I. Balberg, and A. Sa'ar, Phys. Rev. B **69**, 155311 (2004); A. Sa'ar, M. Dovrat, J. Jedrzejewski, and I. Balberg, Physica E **38**, 122 (2007).
[7] P. D. J. Calcott, K. J. Nash, L. T. Canham, M. J. Kane, and D. Brumhead, J. Phys.: Condens. Matter **5**, L91 (1993).
[8] F. A. Reboredo, A. Franceschetti, and A. Zunger, Appl. Phys. Lett. **75**, 2972 (1999); Phys. Rev. B **61**, 13073 (2000).
[9] T. Takagahara and K. Takeda, Phys. Rev. B **53**, R4205 (1996).
[10] L. J. Chen, J. Mater. Chem. **17**, 4639 (2007).
[11] D. D. D. Ma, C. S. Lee, F. C. K. Au, S. Y. Tong, and S. T. Lee, Science **299**, 1874 (2003); R. Q. Zhang, Y. Lifshitz, and S.-T. Lee, Adv. Mater. **15**, 635 (2003).
[12] C. P. Li, X. H. Sun, N. B. Wong, C. S. Lee, S. T. Lee, and B. K. Teo, Chem. Phys. Lett. **365**, 22 (2002).
[13] M. Dovrat, N. Arad, X.-H. Zhang, S.-T. Lee, and A. Sa'ar, Phys. Rev. B **75**, 205343 (2007).
[14] A. R. Guichard, D. N. Barsic, S. Sharma, T. I. Kamins, and M. L. Brongersma, Nano Lett. **6**, 2140 (2006).
[15] D. P. Yu, Z. G. Bai, J. J. Wang, Y. H. Zou, W. Qian, J. S. Fu, H. Z. Zhang, Y. Ding, G. C. Xiong, L. P. You, J. Xu, and S. Q. Feng, Phys. Rev. B **59**, R2498 (1999); A. K. Singh, V. Kumar, R. Note, and Y. Kawazoe, Nano Lett. **5**, 2302 (2005).
[16] M. Zacharias, J. Heitmann, R. Scholz, U. Kahler, M. Schmidt, and J. Blasing, Appl. Phys. Lett. **80**, 661 (2002); V. Vinciguerra, G. Franzo, F. Priolo, and F. I. C. Spinella, J. Appl. Phys. **87**, 8165 (2000).
[17] For short period SiNC superlattices, we have found additional, nondispersive exponential term that is related to intralayer recombination. This phenomenon will be discussed elsewhere.
[18] S. A. Crooker, T. Barrick, J. A. Hollingsworth, and V. I. Klimov, Appl. Phys. Lett. **82**, 2793 (2003).
[19] K. Leung and K. B. Whaley, Phys. Rev. B **56**, 7455 (1997).
[20] E. Martin, C. Delerue, G. Allan, and M. Lannoo, Phys. Rev. B **50**, 18258 (1994); S. Öğüt, J. R. Chelikowsky, and S. G. Louie, Phys. Rev. Lett. **79**, 1770 (1997).
[21] We notice that most models for SiNCs (e.g., Refs. 8, 9, 18, and 19) assume hydrogen terminated surface of the nanocrystals. Yet, we expect the basic symmetries of oxygen terminated SiNCs to be very similar despite that, qualitatively the spectrum of energy levels can be affected by surface termination; see A. Sa'ar, Y. Reichman, M. Dovrat, D. Krapf, J. Jedrzejewski, and I. Balberg, Nano Lett. **5**, 2443 (2005).
[22] K. J. Nash, P. D. J. Calcott, L. T. Canham, and R. J. Needs, Phys. Rev. B **51**, 17698 (1995).
[23] N. Daldosso, M. Luppi, S. Ossicini, E. Degoli, R. Magri, G. Dalba, P. Fornasini, R. Grisenti, F. Rocca, L. Pavesi, S. Boninelli, F. Priolo, C. Spinella, and F. Iacona, Phys. Rev. B **68**, 085327 (2003).
[24] M. Jones, S. Kumar, S. S. Lo, and G. D. Scholes, J. Phys. Chem. C **112**, 5423 (2008).
[25] J. X. Cao, X. G. Gong, J. X. Zhong, and R. Q. Wu, Phys. Rev. Lett. **97**, 136105 (2006); R. Rurali, B. Aradi, Th. Frauenheim, and A. Gali, Phys. Rev. B **76**, 113303 (2007); F. Trani, G. Cantele, D. Ninno, and G. Iadonisi, *ibid.* **72**, 075423 (2005).
[26] M. Bruno, M. Palummo, A. Marini, R. Del Sole, and S. Ossicini, Phys. Rev. Lett. **98**, 036807 (2007); J. Li and A. J. Freeman, Phys. Rev. B **74**, 075333 (2006); L. Yang, C. D. Spataru, S. G. Louie, and M. Y. Chou, *ibid.* **75**, 201304(R) (2007).
[27] The ratio $K/\Delta J$ is essentially independent of the size of the nanostructures and therefore can be considered as a characteristic of the dimensionality of the nanostructures.
[28] A. Franceschetti, L. Wang, H. Fu, and A. Zunger, Phys. Rev. B **58**, R13367 (1998); H. Fu, L.-W. Wang, and A. Zunger, *ibid.* **59**, 5568 (1999).